Research Square

Preprints are preliminary reports that have not undergone peer review.
They should not be considered conclusive, used to inform clinical practice,
or referenced by the media as validated information.

# Utilizing 4D-STEM to Characterize Diffusion-Induced Grain Boundary Migration in NiCr Alloys

**Eitan Hershkovitz**
Pacific Northwest National Laboratory
**Karen Kruska**
Pacific Northwest National Laboratory
**Pauline Simmonnin**
Pacific Northwest National Laboratory
**Konnor Walter**
University of Michigan
**Emmanuelle Marquis**
University of Michigan
**Daniel Schreiber**
Pacific Northwest National Laboratory
**Chongmin Wang**
Chongmin.Wang@pnnl.gov
Pacific Northwest National Laboratory

**Article**

**Keywords:**

**Posted Date:** June 26th, 2026

**DOI:** https://doi.org/10.21203/rs.3.rs-10084719/v1

**License:** This work is licensed under a Creative Commons Attribution 4.0 International License.
Read Full License

**Additional Declarations:** No competing interests reported.

**Version of Record:** A version of this preprint was published at npj Materials Degradation on September 5th, 2026. See the published version at https://doi.org/10.1038/s41529-026-00876-8.

# Abstract

Alloy degradation poses a significant challenge to the safe and reliable performance of alloys in advanced energy systems. Ni-Cr alloys are quite durable in these aggressive conditions but can become susceptible to intergranular oxidation and cracking when subjected to high temperature (300–400°C) oxidizing conditions and stress. Selective oxidation of Cr has been observed to coincide with accelerated grain boundary diffusion and associated diffusion-induced grain boundary migration (DIGM). In these systems, DIGM is characterized by localized Cr depletion and Ni enrichment in the wake of 10s to 100s of nm of lateral grain boundary migration that can extend several micrometers beneath the alloy surface or ahead of propagating crack tips. While it has been established this Cr depletion can impact further corrosion behavior, it is less clear how it affects local mechanical behavior. In this work we use 4-dimensional scanning transmission electron microscopy (4D-STEM) to analyze the impact of DIGM on the local microstructure changes around degraded grain boundaries. By integrating 4D-STEM with elemental analysis via energy dispersive X-ray spectroscopy (EDS), we establish correlations between structural and compositional changes within the DIGM-zones. At low Cr concentrations (5 at.% Cr), compositional changes are insufficient to generate significant coherency strain, whereas at high Cr concentrations (~ 30 at.% Cr), the resulting strain can not only be anisotropic but also exceed what compositional changes alone predict.


# Introduction

The long-term resilience of metal alloys in harsh environments is critical for the sustained and future use of advanced power systems to meet ever increasing energy demands.[1,2] NiCr alloys, due to having excellent mechanical properties, thermal stability, and corrosion resistance,[3] are one of the primary metal alloys that meet the challenges of current and future power generating systems. Despite their general corrosion resistance, NiCr alloys remain susceptible to localized, intergranular corrosion and stress corrosion cracking (SCC) upon exposure to high-temperature (~ 280–330°C) hydrogenated water found in commercial light water reactors (LWRs).[4–8] With sufficient Cr concentrations ( > ~ 21 at.%), NiCr alloys natively form a protective surface oxide layer that inhibits intergranular oxidation .[9] High Cr concentration alloys, like the 30 at.% Cr Alloy 690, are therefore highly resistant to intergranular oxidation and SCC. However, this surface passivation is facilitated by enhanced diffusion of Cr along grain boundaries (GBs) that can lead to local Ni enrichment and Cr depletion with concomitant GB migration.[10–12] This newly formed Cr-depleted region has been shown to be susceptible to corrosive attack if the passivating surface oxide is breached.[13]

Underpinning this severe Cr depletion and localized corrosion susceptibility is the phenomenon of diffusion induced grain boundary migration (DIGM), which has broadly been attributed to the difference in diffusivities of solute and solvent atoms near the GB, as well as to coherency strain energy from solute incorporation.[14–17] Although DIGM in NiCr-based alloys has been studied previously,[10,18] many questions remain regarding its role in driving the further degradation and SCC susceptibility of affected grain

boundaries. Moreover, the impact of secondary factors (e.g., Cr concentration, environment type, temperature, and strain and deformation) has yet to be correlated with changes in DIGM features. As temperature strongly affects diffusion mechanisms and rates, temperature is expected to strongly influence the characteristics of DIGM. For example, Cr diffusion along GBs is dominant over bulk diffusion in Ni-base alloys at moderate operating temperatures (300°C-600°C)[19,20]. As Cr is selectively oxidized over the more noble Ni matrix, the combination of Cr GB diffusion and selective surface Cr oxidation is also expected to result in the formation and injection of vacancies that further accelerate GB diffusion and GB migration.[16,21,22] At higher temperatures (> 600°C), where bulk diffusion is possible, both GB and bulk diffusion, and potentially internal oxidation, must be taken into account.[23]

It has been theorized that DIGM induces strain along the GB.[14,15] The coherency strain model developed by Hillert predicts that strain arises within the DIGM-zone, the region traversed by the migrated GB, because the compositionally altered region remains constrained by the surrounding bulk material of the parent grain.[17] Furthermore, because the GB in DIGM is solid and capable of transmitting stress between crystals, elastically anisotropic compatibility stresses may exist to different extents in the two grains, potentially producing an asymmetric strain state across the boundary.[16] However, the exact details on this DIGM induced strain landscape are unknown.

A deeper understanding of the DIGM process in NiCr alloys requires spatially resolved characterization of compositional and structural changes within and along the DIGM zone. Scanning electron microscopy (SEM), while useful for macroscopic analysis of grain boundaries, lacks the spatial resolution needed to provide atomic-level detail.[9,24,25] Higher resolution characterization techniques like atom probe tomography (APT) and scanning transmission electron microscopy (STEM) are more successful in probing DIGM mechanics. APT has generated high spatial resolution 3D elemental maps of DIGM affected GBs, but cannot provide precise structural information, such as changes in the crystal lattice including the effect of vacancy populations within the DIGM zone.[8,9,12,26,27] Complementary STEM techniques, particularly high angular annular dark field (HAADF) STEM, offer atomic resolution imaging for direct structural measurements, but are still limited in their field of view to tens of nanometers, making large scale, statistically robust quantification challenging. This limited field of view is a significant obstacle when studying DIGM, which can extend 10s of micrometers into the alloy.[28]

To address these challenges, this study leverages 4-dimensional STEM (4D-STEM) to extract large scale, spatial resolved structural information surrounding Ni-Cr alloy GBs that experienced DIGM from high-temperature selective oxidation. In 4D-STEM, an electron probe is rastered across the sample, capturing a 2D reciprocal space diffraction pattern at each 2D real space scan position, hence the “4D” nomenclature.[29] For this work, we employ a specific 4D-STEM technique, scanning electron nanobeam diffraction, to collect nanobeam electron diffraction (NBED) patterns at each scan point.[30] These NBED patterns contain site-specific structural information, enabling the creation of strain maps over large areas of DIGM-zones. By correlating 4D-STEM strain maps with elemental analysis from the same

regions using energy dispersive x-ray spectroscopy (EDS), we bridge the gap between structural attributes and elemental composition in regions affected by DIGM.[22]

## Results

Here, we present data from NiCr binary alloys oxidized at moderate temperatures relevant to energy systems that have been known to illicit DIGM. Specifically, Ni-5Cr and Ni-30Cr samples were exposed to hydrogenated pressurized water (330°C, 100 hr), and a Ni-30Cr sample was oxidized in air (600°C, 160 min). These compositions and environments allow DIGM behavior to be compared across chromium content and oxidizing conditions. More details on the materials and exposure conditions are provided in the separate methods section.

# Effect of Cr concentration on water exposed alloys

Figure 1 shows HAADF-STEM images of the GBs and EDS maps of the DIGM-zones for the Ni-5Cr and Ni-30Cr alloys exposed to 330°C hydrogenated pressurized water in a stainless steel autoclave for 100 h. These exposed samples will be referred to as Ni5Cr-Water and Ni-30Cr-Water, respectively. The original sample surfaces are parallel to the top edge of the images in Figs. 1(a) and 1(f). Dark contrast in the HAADF image corresponds to lower Z oxides regions, lighter contrast corresponds to higher Z metallic regions. The Ni5Cr sample exhibits intergranular oxidation, while the Ni-30Cr sample shows a thin oxide above the grain boundary and no penetrative attack. The white dashed boxes in Figs. 1(a) and 1(f) denote the areas from which the EDS data in Figs. 1(b-e) and 1(g-j) were collected, respectively. The EDS data confirm that both samples formed Cr-rich oxides while the alloy GB has migrated and formed a Cr-depleted region from DIGM, as seen in the Cr maps (Figs. 1(d) and 1(i)). The original grain boundary (OGB) and the migrated grain boundary (MGB) are marked in the Ni EDS maps by a dashed orange line and solid white line, respectively. In the EDS maps we can see that in the Ni30Cr-Water sample, the DIGM-zone at this GB extends deeper into the sample, over a micrometer, while in the Ni5Cr-Water sample, the DIGM-zone visible in EDS extends at least a few hundred nanometers at this GB.

Quantitative EDS composition line scans, extracted from the white dashed boxes and arrows in the Cr EDS maps in Fig. 1, are shown in Fig. 2. These line scans highlight the compositional differences of the DIGM-zones for each alloy. The amount of Ni enrichment and Cr depletion between the two samples differ significantly with Cr depleting from 5 at.% to just 1 at.% in the DIGM-zone of the Ni5Cr-Water sample and from 30 at.% Cr to 16 at.% in the Ni30Cr-Water sample. Similar Cr depletion and DIGM have been observed in Ni5Cr and Ni30Cr alloys under comparable conditions.[9,10] For Ni30Cr in hydrogenated water, deeper depletion has been reported, though at significantly longer exposure times (1000 h vs. 100 h in this study).[13]

4D-STEM was used to ascertain the impact of DIGM on the local strain and structure of the corroded alloys. Figure 3 compares the strain results extracted from the 4D-STEM measurements across the DIGM-zones of the Ni5Cr-Water and Ni30Cr-Water samples. The dashed red boxes in Figs. 1(a) and 1(f)

highlight the locations of the 4D-STEM scans, with data shown in Fig. 3. Figures 3(a) and 3(d) show the reconstructed virtual annular darkfield (VADF) images for the Ni-30Cr-Water and Ni5Cr-Water samples, and local strain measurements in panels (b, c) and (e, f). The local strain was calculated for each sample by measuring the distance between diffraction reflections in each diffraction pattern collected at each 4D-STEM scan position. A reference region far from the GB, but still within the scan area, was used as the unstrained reference for the resulting strain maps. As such, the resulting strain maps visualize relative strain percent not absolute lattice parameter measurements. An inset showing a single diffraction pattern outlined in white, with the zone axis of the respective grain, is provided for reference. As a guide for the reader, the OGB and MGB are again marked by dashed orange and solid white lines, respectively. It is important to note that areas on the opposite side of the MGB belong to the adjacent grain and are no longer aligned with the current zone axis, rendering strain values from those regions invalid for analysis.

Examining the strain maps in Figs. 3(b) and (c), we observe lattice contraction (denoted by blue coloring) within the DIGM-zone of the Ni30Cr-Water sample, with the onset of this contraction appearing relatively sharp. Conversely, the DIGM zone of the Ni5Cr-Water sample appears relatively strain free, with no significant measured strain visible in the strain maps shown in Figs. 3(e) and (f). These observations are further supported by violin plots of individual strain datapoints, shown in Fig. 3(g), comparing the measured strain inside and outside the DIGM-zone for both alloys. For the Ni30Cr-Water we find a significant difference, roughly 1%, in measured compressive strain inside the DIGM-zone compared to outside for $\epsilon_{11}$ (-1.140 ± 0.620% vs. -0.010 ± 0.453%) while $\epsilon_{22}$ differed only slightly, roughly 0.2%, inside the DIGM-zone compared to outside (-0.245 ± 0.675% vs. -0.013 ± 0.715%). Comparatively, the measured difference in Ni5Cr-Water is much smaller, roughly 0.1%, for compressive strain inside the DIGM zone compared to outside for both components: $\epsilon_{11}$ (-0.148 ± 0.525% vs. -0.056 ± 0.507% and $\epsilon_{22}$ (-0.136 ± 0.509% vs. -0.024 ± 0.522%).

We can further compare the measured strain with that expected from the composition change between each sample's bulk and its respective DIGM-zone using our EDS data (Fig. 2). During DIGM, the local composition near the GB changes compared to the bulk value, and this compositional change should produce a corresponding lattice strain. Based on reported NiCr lattice parameters versus composition, the Ni5Cr-Water sample has an expected strain of roughly − 0.110%, which matches our measurement and indicates that strain in this DIGM-zone is primarily attributed to the composition change.[31] In contrast, the DIGM-zone in the Ni30Cr-Water sample has an expected compositional strain of -0.668%.[31] The larger compressive strain measured in the DIGM-zone, particularly $\epsilon_{11}$ perpendicular to the GB, cannot only be explained by composition change within the DIGM-zone. Notably in the opposite grain there is no measured strain across from the DIGM zone as seen in supplementary Figure S1.

## Less Cr depletion and larger DIGM zones in high temperature air exposure

A Ni30Cr alloy was oxidized in air at 600°C for 160 min using a box furnace to investigate the role of temperature regimes where bulk diffusion becomes significant in influencing DIGM behavior. This sample will be referred to as Ni30Cr-Air. Figure 4 shows a HAADF-STEM image of the GB and EDS analysis of the DIGM-zone in the Ni30Cr-Air sample. The oxidation resulted in a qualitatively similar Cr-rich surface oxide layer and Cr-depleted DIGM zone in the underlying alloy as the Ni30Cr-Water sample. In Fig. 4(a), the white dashed box denotes the EDS scan area shown in Figs. 4(b-e), while the dashed red box denotes the location of the 4D-STEM scan, with corresponding data shown in Fig. 5. In the Ni EDS map (Fig. 4(c)), the OGB and MGB are marked with dashed orange and solid white lines respectively while a white dashed box and arrow in the Cr EDS map (Fig. 4(d)) indicate the location of the line scan presented in Fig. 4(f). The EDS line scan (Fig. 4(f)) reveals quantitative Cr depletion in the DIGM zone to ~ 20 at.% from ~ 28 at.% in the surrounding matrix.

Examining the strain environment of the Ni30Cr-Air DIGM-zone in Fig. 5 reveals further similarities to the Ni30Cr-Water sample. The strain maps in Figs. 5(b) and (c) display lattice contraction within the DIGM-zone, bounded by the dashed orange line (OGB) and solid white line (MGB) in Fig. 5(a). As with the Ni30Cr-Water sample, lattice contraction is observed upon entering the DIGM-zone, as highlighted by the violin plots in Fig. 5(d) where we find a difference of roughly 0.5% in measured compressive strain inside the DIGM-zone compared to outside for both components: $\epsilon_{11}$ (-0.632 ± 0.560% vs. -0.112 ± 0.607% and $\epsilon_{22}$ (-0.536 ± 0.371% vs. -0.108 ± 0.407%). This is only slightly larger than the expected strain, -0.431%, from the compositional difference measured inside and outside the DIGM-zone (Fig. 4.). Additionally, the anisotropic nature of the strain seen in the Ni30Cr-Water sample is not present in the Ni30Cr-Air sample with both $\epsilon_{11}$ and $\epsilon_{22}$ being within 0.1% of each other. Like the previous samples the Ni30Cr-Air sample exhibited no strain in the grain opposite the DIGM-zone as seen in supplementary Figure S1.

# Discussion

Our results provide critical insight into the effects of both initial alloy composition and exposure temperature on the behavior of DIGM in NiCr alloys. We demonstrate that DIGM-induced strain is confined exclusively to the compositionally altered DIGM-zone, with no measurable strain in the adjacent grain across the boundary. Composition plays a decisive role with the Ni5Cr alloy sample producing insufficient compositional change to generate measurable strain, while the Ni30Cr samples exhibit strain whose magnitude and anisotropy depend on exposure conditions. These observations reveal a strain landscape governed by the interplay between composition and temperature.

The confinement of strain exclusively within the DIGM-zone is consistent with the coherency strain model, in which elastic strain arises because the compositionally altered layer remains constrained by the surrounding bulk of the parent grain.[16,17] As observed in Supplementary Figure S1, the adjacent grain on the other side of the boundary exhibits no measurable strain, confirming that the strain originates from the compositional misfit within the de-alloyed region rather than from mechanical effects transmitted broadly across the boundary. This asymmetry is expected; only the DIGM-zone has undergone a composition change relative to its constraining matrix, while the neighboring grain retains

its original composition and therefore experiences no misfit with itself. Critically, the Ni30Cr-Water and Ni5Cr-Water samples underwent identical exposure conditions, isolating the effect of initial alloy composition on the resulting strain landscape. The two compositions differ fundamentally in their oxidation response. The Ni5Cr-Water sample cannot form a sufficient passivation layer, leading to the formation of a penetrative oxide within the GB, while the Ni30Cr-Water sample develops a fully formed self-passivating layer at the surface as observed in Fig. 1(f) with no penetrative oxide. As such the compositional change in the DIGM-zone produced by Cr depletion in the Ni5Cr-Water sample is insufficient to generate measurable strain. This is consistent with Hillert's formulation, in which coherency strain energy scales with the square of the composition difference, meaning that small compositional changes produce disproportionately small strain.[17] In contrast, the Ni30Cr-Water sample, with a much larger Cr reservoir available for depletion, produces a far greater compositional change, and therefore a larger misfit between the DIGM-zone and its constraining parent grain.

Additionally, we observe an anisotropic nature in the strain measured within the Ni30Cr-Water DIGM-zone, with increased $\epsilon_{11}$ compared to $\epsilon_{22}$. This anisotropy is inconsistent with strain arising solely from Cr vacancies in a cubic symmetry system, which would be expected to produce isotropic volumetric contraction.[32] Instead, the preferential strain perpendicular to the boundary plane is directly consistent with the volume change mechanism described by Balluffi and Cahn.[14] They established that unequal GB diffusion during DIGM produces a net addition or removal of atoms form the alloyed or de-alloyed zone, which in turn results in volumetric expansion or contraction specifically in the direction perpendicular to the boundary plane.[14] In the present work, the preferential diffusion of Cr out of the DIGM-zone along the grain boundary, driven by the selective oxidation at the surface, produces a net removal of atoms whose volume change is primarily in the direction normal to the boundary. This directional nature of the atomic flux, rather than an isotropic volumetric effect, produces the observed anisotropic strain state.

Furthermore, the strain measured in the Ni30Cr-Water DIGM-zone significantly exceeds what can be attributed to the lattice parameter change from composition alone (based on the NiCr lattice parameter as a function of Cr concentration).[31] This excess strain suggests additional contributions beyond simple compositional misfit, and is consistent with previous DIGM analyses in Ni-Cr from molten salt corrosion.[22] The grain boundary dislocation (GBD) climb model proposed by Balluffi and Cahn provides one possible explanation.[14] DIGM involves the climb of GBDs driven by vacancy flux divergences from unequal grain boundary diffusivities of solute and solvent atoms.[14] At 330°C, the matrix self-diffusion distance of Cr and Ni approaches only 5 pm after 100 hours, indicating that the grain boundary is migrating orders of magnitude faster than bulk diffusion can accommodate.[33] Under these conditions, the defects generated by the GBD climb mechanism or excess vacancies produced by flux divergences during boundary migration would lack sufficient bulk mobility to anneal, potentially remaining frozen within the DIGM-zone and contributing measurable strain beyond the compositional misfit.[14] We note that directly resolving dislocation densities within the DIGM zone is complicated by the nanoscale width of the region and the overlapping strain fields from compositional gradients, and remains an avenue for future work.

Interestingly, the Ni30Cr-Air DIGM-zone does not exhibit the same strain anisotropy as the Ni30Cr-Water sample, and its measured strain is close to what composition alone predicts. We observe the Cr concentration within the Ni30Cr-Air DIGM-zone decreased by approximately 10 at.% relative to the bulk (Fig. 4(f)), compared to a decrease of roughly 14 at.% in the Ni30Cr-Water sample (Fig. 2(b)). Despite an exposure time over an order of magnitude shorter, the Ni30Cr-Air DIGM-zone is substantially larger than the Ni30Cr-Water counterpart yet exhibits less Cr depletion within the zone, indicating that exposure time is not the primary factor governing either the extent of grain boundary migration or the compositional change within the zone.

Instead, the higher temperature (600°C) fundamentally alters both the diffusion landscape and the capacity for strain relaxation. At 600°C, the self-diffusion distance of Cr and Ni approaches 5 nm in 160 minutes, which is still small enough that the GB migrates faster than bulk diffusion can fully follow, though we note that excess vacancies introduced by the migrating boundary may locally enhance matrix diffusion beyond equilibrium predictions.[33] Nevertheless, bulk diffusion at this temperature is no longer negligible relative to grain boundary transport, which may partially homogenize the DIGM-zone through backfilling.[34] Alternatively, or even additionally, the faster moving boundary at 600°C may sweep into fresh material before it can fully deplete, limiting the compositional change at any given point along the migration path. In either case, the net compositional change within the DIGM-zone is less than in the Ni30Cr-Water sample, directly reducing the coherency strain energy, which scales with the square of the composition difference.[17] In addition, if excess point defects are generated during the DIGM process through GBD climb and vacancy flux divergences, the significantly enhanced bulk diffusion at 600°C would provide pathways for their annihilation, unlike at 330°C, where the near-zero bulk diffusivity (5 pm diffusion distance in 100 hours) would effectively freeze any such defects into the DIGM-zone.[14] However, with the present data, we cannot definitively separate the contributions of reduced compositional misfit, differences in boundary migration rate, zone geometry, and potential defect annealing.

The transition from anisotropic to isotropic strain between the two Ni30Cr samples is also consistent with the change in diffusion conditions at higher temperature. At 330°C, where bulk diffusion is essentially frozen, the volume change associated with net atom removal through unequal grain boundary diffusion is confined to direction perpendicular to the boundary plane, producing the observed anisotropy.[14] However, at 600°C, enhanced bulk diffusion enables a more uniform redistribution of atoms within and around the DIGM-zone, reducing the directional dominance of the grain boundary flux channel. The volume change is no longer confined to the perpendicular direction but can be accommodated more isotopically through bulk transport pathways. Furthermore, the substantially thicker DIGM-zone in the Ni30Cr-Air sample (i.e., the greater distance from the original to the migrated grain boundary position) distributed any residual volume change over a larger region, further shrinking any anisotropic signature. The convergence of measured strain toward the compositional prediction is thus consistent with a regime where enhanced bulk diffusion homogenizes the strain response and defect-related contributions have largely relaxed. While the correlation between diffusion regime,

temperature-dependent relaxation, and the observed strain characteristics is strongly supported by our measurements, direct quantification of the individual contributions from coherency strain, directional flux effects, and defect accumulation warrants further investigation through complementary techniques such as in-situ heating TEM experiments to monitor strain evolution during controlled annealing.

The use of 4D-STEM to construct strain maps over large areas surrounding DIGM-zones proved to be a powerful method for capturing localized strain effects induced by DIGM. This technique enabled precise structural characterization at sub-micron length scales, revealing strain trends inaccessible with conventional STEM imaging methods. Future research should aim to directly confirm the role of defect accumulation through complementary techniques such as weak-beam dark-field imaging to assess dislocation densities within DIGM-zones, and in-situ heating TEM experiments to separate compositional strain from defect-related contributions by monitoring strain evolution during controlled annealing. Additionally, the study of DIGM-induced strain should be expanded to more complex alloys that better reflect real world conditions, including commercial alloys and alloys containing crack tips, where the interplay between DIGM, localized strain, and mechanical integrity may have significant implications for long term grain boundary stability.

## Conclusion

In this study, 4D-STEM strain mapping combined with EDS elemental analysis clarified the strain landscape associated with DIGM in NiCr alloys exposed to varying compositions and temperatures. We found that DIGM-induced strain is confined exclusively to the compositionally altered DIGM-zone, with no measurable strain detected in the adjacent grain across the boundary, consistent with the coherency strain model in which misfit between the de-alloyed layer and its constraining parent grain is the origin of elastic strain. In the Ni5Cr alloy, the compositional change produced by DIGM is insufficient to generate measurable strain, consistent with the predicted quadratic scaling of coherency strain energy with composition difference. In contrast, the Ni30Cr alloys exhibit clearly measurable strain whose magnitude, anisotropy, and relationship to compositional predictions depend strongly on exposure temperature. At lower temperature (330°C), the observed anisotropic strain is consistent with the directional volume change produced by unequal atomic fluxes during grain boundary diffusion and manifested as preferential contraction normal to the boundary plane. The measured strain significantly exceeds what can be attributed to lattice parameter changes from composition alone, suggesting additional contributions (e.g., defects generated by grain boundary dislocation climb) are also present. At higher temperature (600°C), strain becomes nearly isotropic and converges toward purely compositional predictions, consistent with enhanced bulk diffusion enabling more uniform redistribution of atoms.

## Methods

# Characterization

TEM sample preparation was performed using a FEI Quanta dual beam Ga Ion FIB/SEM. HAADF-STEM imaging was performed using an aberration-corrected Spectra (Thermo Fisher)

microscope. The accelerating voltage of the microscope was 300 keV, and the semi-convergence angle was 30 mrad. EDS data was collected with a 300 pA probe and a dwell time of 20 µs. 4D-STEM was performed at 300 keV with an electron probe semi-convergence angle of 1.06 mrad and a full width at half-maximum probe size of roughly 1.5 nm. The electron probe was formed in microprobe mode with a 50-µm condenser aperture. 4D-STEM data was recorded with the electron microscope pixel array detector.[35] The exit-wave power-cepstrum method for strain mapping described by Padgett *et al* was used in this work in addition to some of the Python functions provided from the Muller Group Cornell Github.[36]. VADF images were generated by applying a digital mask to each diffraction pattern in the 4D-dataset and summing the intensity under the mask to mimic the effect of a physical annular dark field detector. Each pixel in the VADF image corresponds to the summed intensity under the digital mask from an individual diffraction pattern.

# Materials

This study focused on binary NiCr alloys to investigate the fundamentals of DIGM under oxidizing conditions at moderate temperatures (300–600°C). Three alloy samples were studied, as detailed in Table 1, which outlines their respective conditions. To isolate and analyze the different

Table 1
Nominal compositions and treatments of the alloys used in this study

| Sample | Composition (at. %) | Exposure Type | Exposure Conditions |
|---|---|---|---|
| Ni5Cr-Water | 95Ni5Cr | Hydrogenated Water | 100 hrs, 330°C, 11cc $H_2$/kg |
| Ni30Cr-Water | 70Ni30Cr | Hydrogenated Water | 100 hrs, 330°C, 11cc $H_2$/kg |
| Ni30Cr-Air | 70Ni30Cr | Air | 160 min, 600°C |

governing conditions of DIGM, we conducted two comparisons: (1) alloys with differing nominal compositions but identical exposure conditions and (2) alloys with identical nominal compositions but differing exposure conditions. Specifically, the Ni5Cr-Water and Ni30Cr-Water samples were exposed to hydrogenated water for 100 hrs at 330°C to examine the effect of Cr concentration on DIGM properties. In contrast, Ni30Cr-Water and Ni30Cr-Air had identical compositions, but the Ni30Cr-Air sample was exposed for 160 min in air at 600°C to evaluate how DIGM behavior changes when bulk diffusion becomes significant at higher temperatures. Further details on the synthesis and exposure treatment of the alloys used in this study can be found in previous literature cited here.[10,37]

# Declarations

# Competing interests

All authors declare no financial or non-financial competing interests.

# Author Contribution

EH and DS conceptualized and designed this study. DS, KK, KW, and EM synthesized the bulk alloy samples and performed exposures. EH prepared all TEM specimens, collected all TEM data, and performed all data processing and analysis. PS performed diffusion calculations. DS and KK contributed to data interpretation. EH wrote the original draft. All authors reviewed and edited the manuscript. DA and CW acquired funding and supervised the research. All authors read and approved of the final manuscript.

# Acknowledgement

This work was supported by the U.S. Department of Energy (DOE) Office of Science, Basic Energy Sciences (BES), Materials Science and Engineering Division, Mechanical Behavior and Radiation Effects program (PNNL FWP 56909). The 4D-STEM work was carried out by using microscopes that are funded in part by a grant from the Washington State Department of Commerce's Clean Energy Fund. The TEM measurements were conducted on a project award (DOI: 10.46936/staf.proj.2016.49687/60006123) from the Environmental Molecular Sciences Laboratory, a DOE Office of Science User Facility sponsored by the Biological and Environmental Research program at Pacific Northwest National Laboratory (PNNL). PNNL is a multiprogram national laboratory operated by Battelle for the U.S. DOE under Contract DE-AC05-79RL01830.

# Data Availability

4D-STEM data sets generated during the current study are not publicly available due to their large size but are available from the corresponding author on request.

## References

1. Cattant, F., Crusset, D. & Féron, D. Corrosion issues in nuclear industry today. *Mater. Today* 11, 32–37 (2008).
2. Scott, P. M. & Combrade, P. General corrosion and stress corrosion cracking of Alloy 600 in light water reactor primary coolants. *J. Nucl. Mater.* 524, 340–375 (2019).
3. Young, D. J. *High Temperature Oxidation and Corrosion of Metals*. (Elsevier, 2008).
4. Bruemmer, S. M. & Was, G. S. Microstructural and microchemical mechanisms controlling intergranular stress corrosion cracking in light-water-reactor systems. *J. Nucl. Mater.* 216, 348–363 (1994).

5. Sennour, M., Laghoutaris, P., Guerre, C. & Molins, R. Advanced TEM characterization of stress corrosion cracking of Alloy 600 in pressurized water reactor primary water environment. *J. Nucl. Mater.* 393, 254–266 (2009).
6. Persaud, S. Y., Korinek, A., Huang, J., Botton, G. A. & Newman, R. C. Internal oxidation of Alloy 600 exposed to hydrogenated steam and the beneficial effects of thermal treatment. *Corros. Sci.* 86, 108–122 (2014).
7. Pande, C. S., Suenaga, M., Vyas, B., Isaacs, H. S. & Harling, D. F. Direct evidence of chromium depletion near the grain boundaries in sensitized stainless steels. *Scr Met. U. S.* 11:8, (1977).
8. Schreiber, D. K., Olszta, M. J. & Bruemmer, S. M. Grain boundary depletion and migration during selective oxidation of Cr in a Ni–5Cr binary alloy exposed to high-temperature hydrogenated water. *Scr. Mater.* 89, 41–44 (2014).
9. Kruska, K., Schreiber, D. K., Olszta, M. J., Riley, B. J. & Bruemmer, S. M. Temperature-dependent selective oxidation processes for Ni-5Cr and Ni-4Al. *Corros. Sci.* 139, 309–318 (2018).
10. Xue, F. & Marquis, E. A. Role of diffusion-induced grain boundary migration in the oxidation response of a Ni-30 Cr alloy. *Acta Mater.* 240, 118343 (2022).
11. Volpe, L., Burke, M. G. & Scenini, F. Oxidation behaviour of solution-annealed and thermally-treated Alloy 690 in low pressure H2-Steam. *Corros. Sci.* 167, 108514 (2020).
12. Weiser, M., Olszta, M. J., Engelhard, M. H., Zhu, Z. & Schreiber, D. K. Visualizing oxygen transport pathways during intergranular oxidation in Ni-Cr. *Npj Mater. Degrad.* 7, 70 (2023).
13. Kruska, K., Olszta, M. J., Wang, J. & Schreiber, D. K. Intergranular corrosion of Ni-30Cr in high-temperature hydrogenated water after removing surface passivating film. *Npj Mater. Degrad.* 8, 1–10 (2024).
14. Balluffi, R. W. & Cahn, J. W. Mechanism for diffusion induced grain boundary migration. *Acta Metall.* 29, 493–500 (1981).
15. Cahn, J. W., Pan, J. D. & Balluffi, R. W. *Diffusion Induced Grain Boundary Migration*. https://www.osti.gov/biblio/6146335 (1979) doi:10.2172/6146335.
16. King, A. H. Diffusion induced grain boundary migration. *Int. Mater. Rev.* 32, 173–189 (1987).
17. Hillert, M. On the driving force for diffusion induced grain boundary migration. *Scr. Metall.* 17, 237–240 (1983).
18. Sahlaoui, H., Sidhom, H. & Philibert, J. Prediction of chromium depleted-zone evolution during aging of Ni–Cr–Fe alloys. *Acta Mater.* 50, 1383–1392 (2002).
19. Basu, S. N. & Halloran, J. W. Tracer isotope distribution in growing oxide scales. *Oxid. Met.* 27, 143–155 (1987).
20. Frischat, G. H. Mass Transport in Solids. *Angew. Chem. Int. Ed. Engl.* 13, 384–398 (1974).
21. Jahn, R. J. & King, A. H. Vacancy deposition during diffusion-induced grain boundary migration. *Philos. Mag. A* 54, L3–L7 (1986).
22. Yang, Y. *et al.* One dimensional wormhole corrosion in metals. *Nat. Commun.* 14, 988 (2023).

23. Wood, G. C., Stott, F. H., Whittle, D. P., Shida, Y. & Bastow, B. D. The high-temperature internal oxidation and intergranular oxidation of nickel-chromium alloys. *Corros. Sci.* 23, 9–25 (1983).
24. Yang, L., Qian, H., Hao, X. & Kuang, W. The effects of grain boundary structure and bulk Cr content on grain boundary degradation behavior of Ni-Cr binary alloys in high temperature CO2. *Acta Mater.* 263, 119496 (2024).
25. Yang, L. *et al.* Grain boundary oxidation behavior of Ni15Cr alloy in high temperature carbon dioxide. *Scr. Mater.* 220, 114935 (2022).
26. Kruska, K. *et al.* Nanoscale characterisation of grain boundary oxidation in cold-worked stainless steels. *Corros. Sci.* 63, 225–233 (2012).
27. Schreiber, D. K., Olszta, M. J. & Bruemmer, S. M. Directly correlated transmission electron microscopy and atom probe tomography of grain boundary oxidation in a Ni–Al binary alloy exposed to high-temperature water. *Scr. Mater.* 69, 509–512 (2013).
28. Langelier, B. *et al.* Effects of boundary migration and pinning particles on intergranular oxidation revealed by 2D and 3D analytical electron microscopy. *Acta Mater.* 131, 280–295 (2017).
29. Ophus, C. Four-Dimensional Scanning Transmission Electron Microscopy (4D-STEM): From Scanning Nanodiffraction to Ptychography and Beyond. *Microsc. Microanal.* 25, 563–582 (2019).
30. Zuo, J.-M. & Tao, J. Scanning Electron Nanodiffraction and Diffraction Imaging. in *Scanning Transmission Electron Microscopy: Imaging and Analysis* (eds Pennycook, S. J. & Nellist, P. D.) 393–427 (Springer, New York, NY, 2011). doi:10.1007/978-1-4419-7200-2_9.
31. Nash, P. The Cr – Ni (Chromium-Nickel) system. *Bull. Alloy Phase Diagr.* 7, 466–476 (1986).
32. The Continuum Theory of Lattice Defects. in *Solid State Physics* vol. 3 79–144 (Academic Press, 1956).
33. Monma, K., Suto, H. & Oikawa, H. Diffusion of Ni63 and Cr51 in Nickel-Chromium Alloys (On the Relation between High-Temperature Creep and Diffusion in Nickel Base Solid Solutions. I). *J. Jpn. Inst. Met.* 28, 188–192 (1964).
34. Was, G. S., Tischner, H. H. & Latanision, R. M. The influence of thermal treatment on the chemistry and structure of grain boundaries in inconel 600. *Metall. Trans. A* 12, 1397–1408 (1981).
35. Tate, M. W. *et al.* High Dynamic Range Pixel Array Detector for Scanning Transmission Electron Microscopy. *Microsc. Microanal.* 22, 237–249 (2016).
36. Padgett, E. *et al.* The exit-wave power-cepstrum transform for scanning nanobeam electron diffraction: robust strain mapping at subnanometer resolution and subpicometer precision. *Ultramicroscopy* 214, 112994 (2020).
37. Bruemmer, S. M., Olszta, M. J., Toloczko, M. B. & Schreiber, D. K. Grain boundary selective oxidation and intergranular stress corrosion crack growth of high-purity nickel binary alloys in high-temperature hydrogenated water. *Corros. Sci.* 131, 310–323 (2018).

# Figures

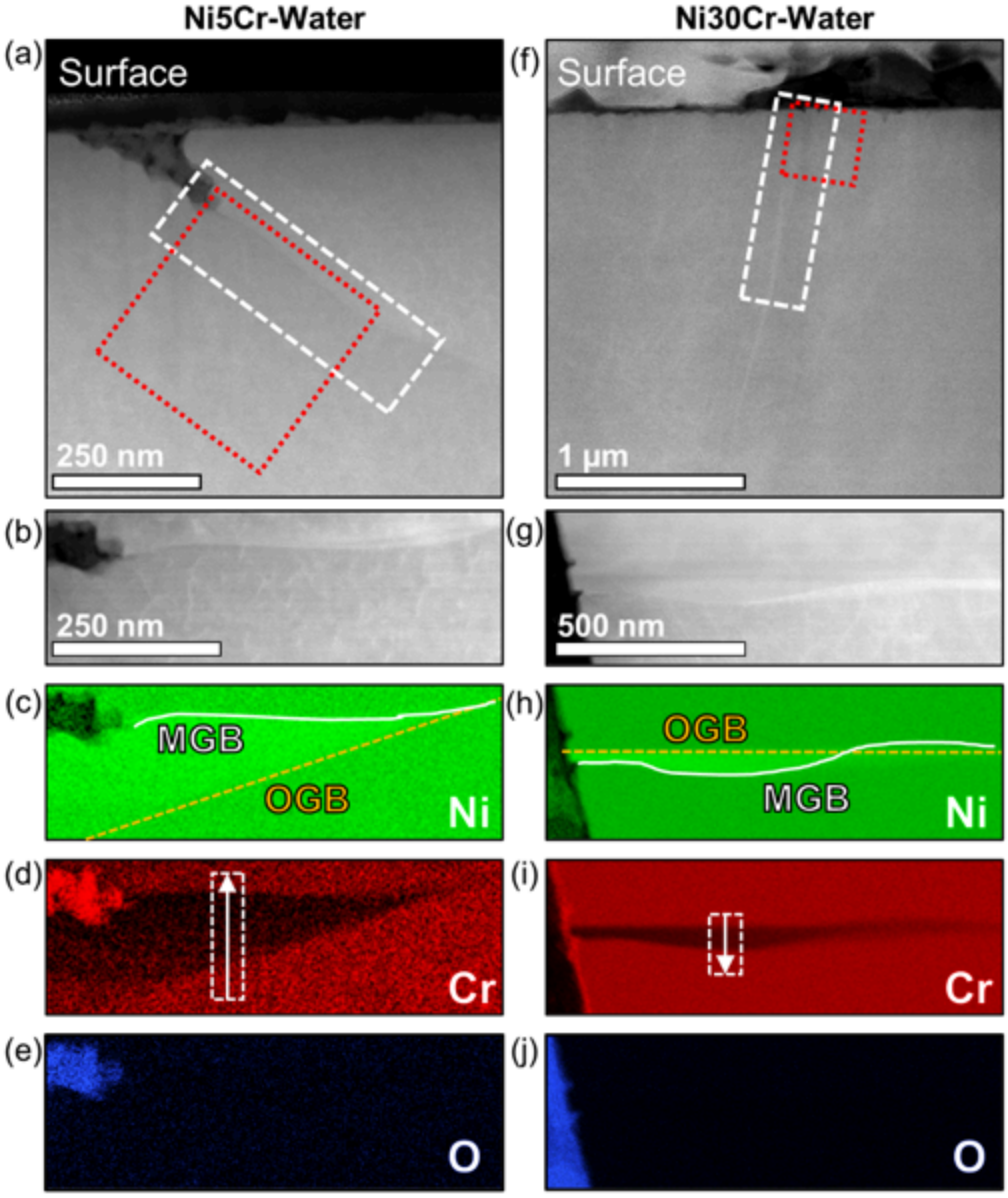



**Figure 1**

HAADF-STEM and EDS of Ni5Cr-Water and Ni30Cr-Water samples. (a-e) HAADF-STEM images and corresponding Ni, Cr, and O EDS maps of the DIGM-zone for the Ni5Cr-Water alloy (a-e) and the Ni30Cr-Water alloy (f-j). The penetrating oxide in the Ni5Cr-Water sample can be seen as the bright red and blue regions in the upper left of the Cr (d) and O (e) EDS maps. The original grain boundary (OGB) and migrated grain boundary (MGB) are indicated by the dashed orange and solid white lines respectively.

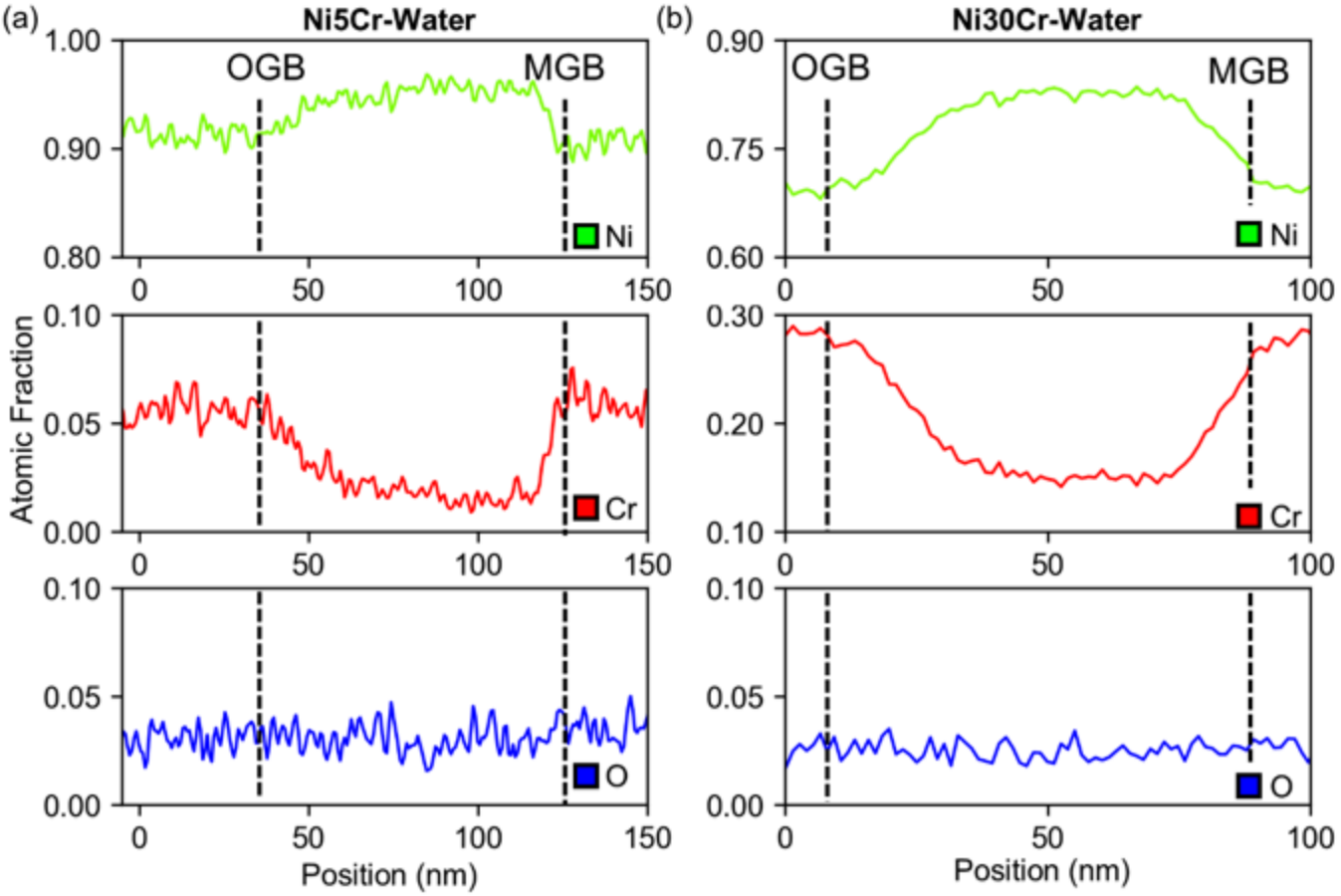



**Figure 2**

Ni, Cr, and O line scans across the DIGM-zone in the Ni5Cr-Water and Ni30Cr-Water samples. Note the difference in atomic fraction scale between the (a) Ni5Cr-Water sample and (b) Ni30Cr-Water sample. The locations of these line scans are marked by the white arrows in Fig. 1.

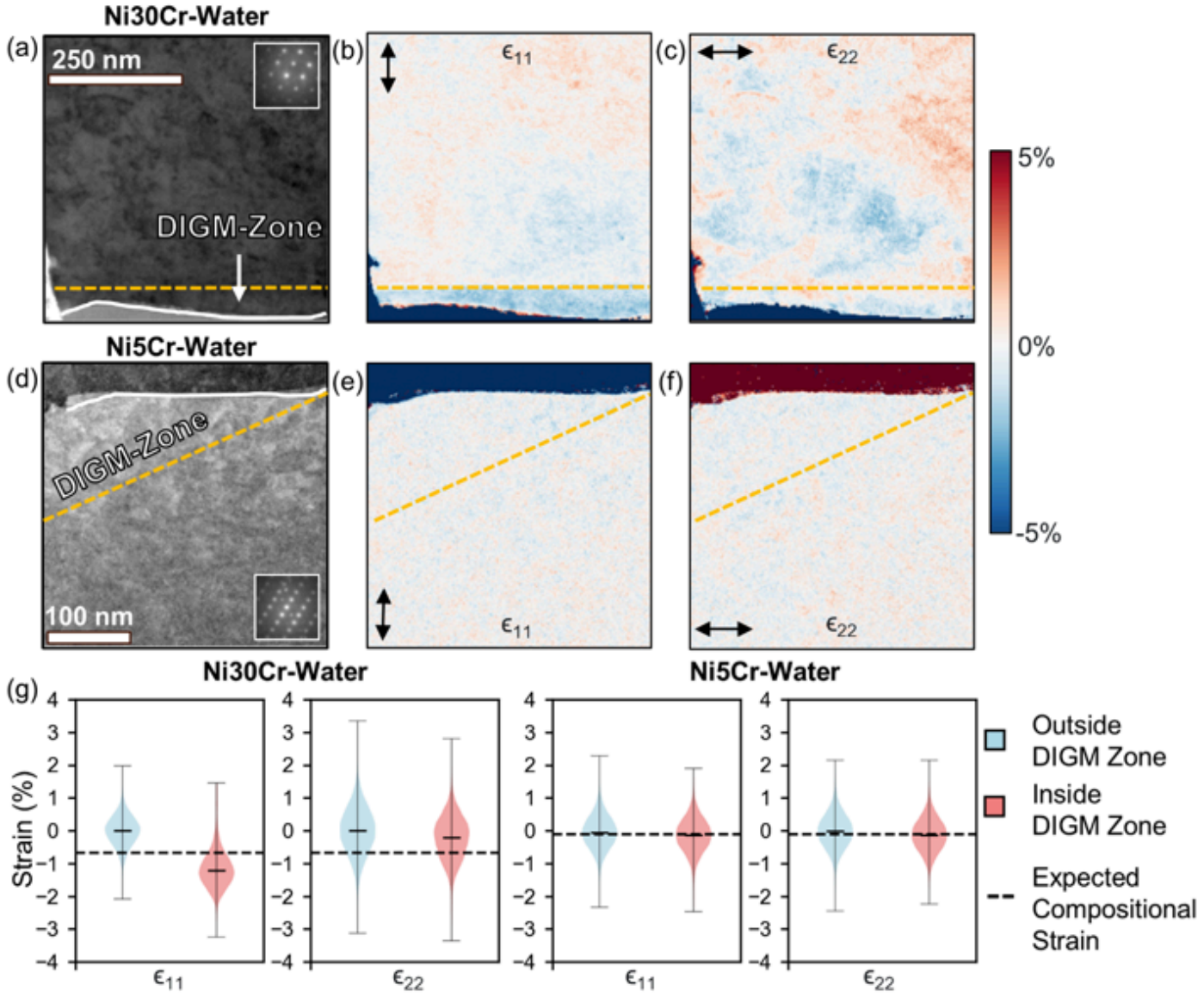



**Figure 3**

4D-STEM strain analysis across the DIGM-zones of the Ni5Cr-Water and Ni30Cr-Water samples. (a) VADF image for the Ni30Cr-Water sample with corresponding strain maps $\epsilon_{11}$ (b) and $\epsilon_{22}$ (c). (d) VADF image for the Ni5Cr-Water sample with corresponding strain maps $\epsilon_{11}$ (e) and $\epsilon_{22}$ (f). Black arrows in (b), (c), (e), and (f) denote the strain measurement direction. The OGB and MGB are marked by the dashed orange and solid white lines respectively, denoting the DIGM zone. (g) Violin plots of the measured strain inside the DIGM zone, red, and outside the DIGM-zone, blue, for both samples with the horizontal dashed black line indicating the expected strain from change in composition into the DIGM-zone

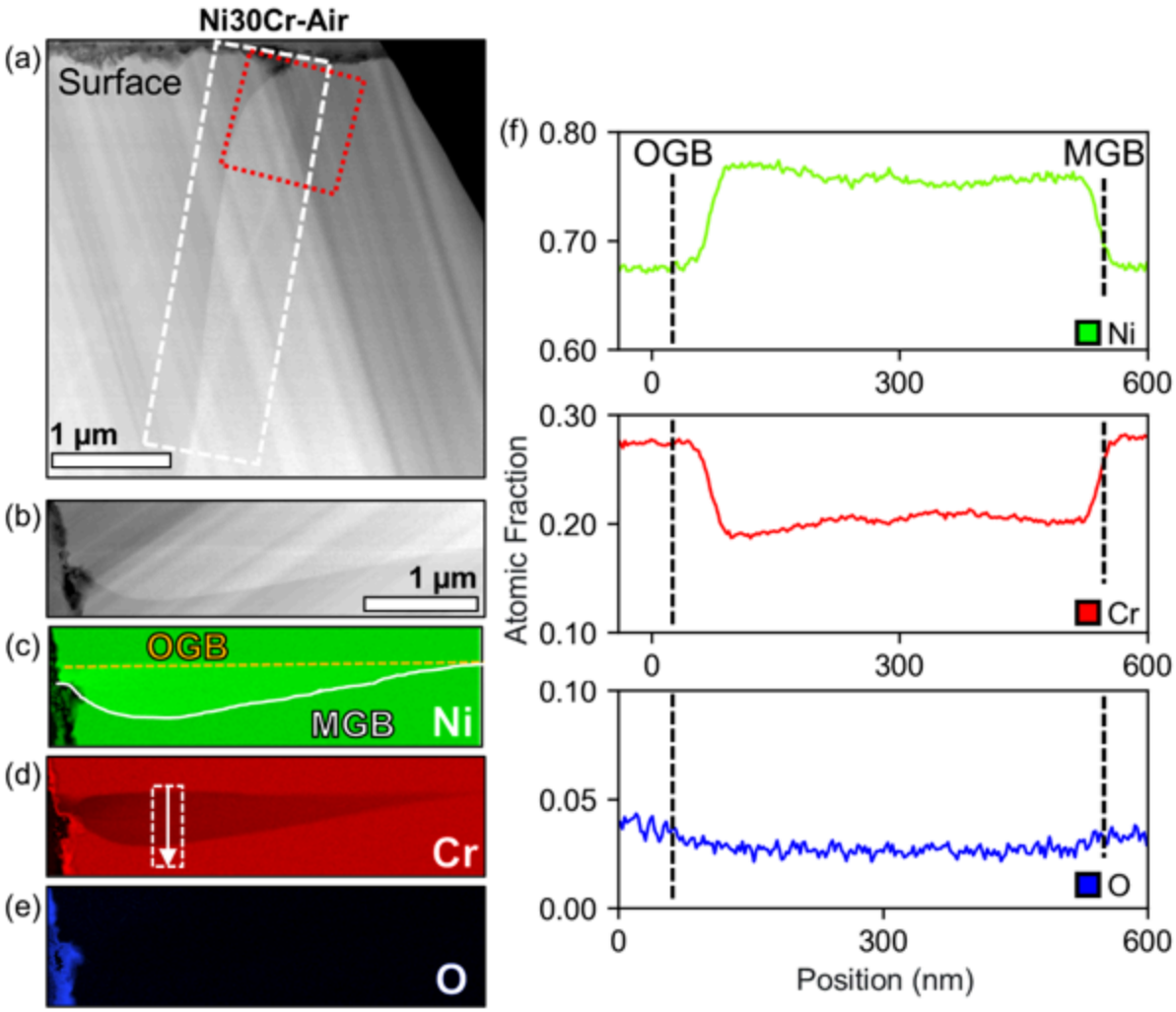



**Figure 4**

HAADF-STEM and EDS overview of the Ni30Cr-Air sample. (a-e) HAADF-STEM images and corresponding Ni, Cr, and O EDS maps of the DIGM-zone. (f) Ni, Cr, and O line profiles taken from the location denoted by the white dashed boxed arrow in (d).

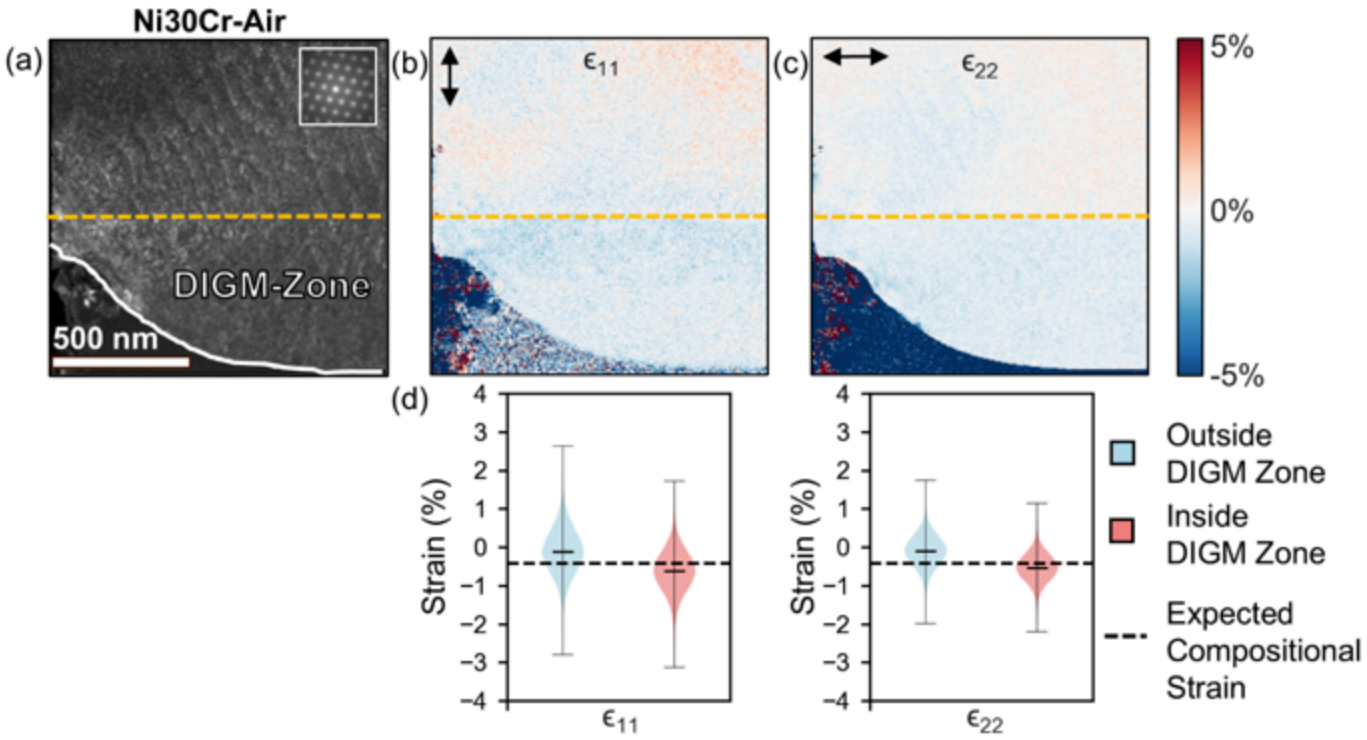



**Figure 5**

4D-STEM strain analysis across the DIGM-zone of the Ni30Cr-Air sample. (a) VADF image for the Ni30Cr-Air sample with corresponding strain maps $\epsilon_{11}$ (b) and $\epsilon_{22}$ (c). Black arrows in (b) and (c) denote the strain measurement direction. (d) The OGB and MGB are marked by the dashed orange and solid white lines respectively, denoting the DIGM-zone. Violin plots of the measured strain inside the DIGM zone, red, and outside the DIGM-zone, blue, for both samples with the horizontal dashed black line indicating the expected strain from change in composition into the DIGM-zone

## Supplementary Files

This is a list of supplementary files associated with this preprint. Click to download.

- V164DSTEMtoNiCrDIGMSI.docx